JOURNAL OF MODERN OPTICS, 2002, VOL. 49, NO. 3/4, 529–537

Parametric downconversion vs optical parametric amplification: a comparison of their quantum statistics

ELNA M. NAGASAKO, SEAN J. BENTLEY, ROBERT W. BOYD*

The Institute of Optics, University of Rochester, Rochester, New York 14627, USA

and GIRISH S. AGARWAL

Physical Research Laboratory, Navrangpura, Ahmedabad-380 009, India

(*Received 23 June 2001*)

Abstract. The extent to which the intense light generated by an unseeded, high-gain optical parametric amplifier retains the desired quantum statistical properties of the individual photon pairs generated by spontaneous parametric downconversion is analysed. It is shown that certain but not all of these properties are retained, with important implications for applications of quantum optics.

1. Introduction

The correlations inherent in quantum states of light have been utilized for low-noise measurements [1]. In recent years this concept has been extended into the realm of imaging [2–7]. In one such proposal, optical parametric oscillators have been used to generate images that exhibit strong nonclassical spatial correlations, allowing noise reduction below the shot-noise limit [8]. A different aspect of quantum imaging has been the use of two-photon entangled states in proposals for the achievement of sub-Rayleigh-limit resolution via configurations that exploit the novel fourth-order interferometric properties of these states [9, 10]. While the interferometric properties of entangled states have been extensively analysed under a variety of arrangements [11–14], these analyses have typically been restricted to states with a single photon in each mode. When input states with more than one photon in each mode are used (e.g. with an unseeded, high-gain optical parametric amplifier), the extent to which these interferometric properties persist has been unclear.

In this paper the various contributions to the output of four-port fourth-order interferometers are analysed, with emphasis on the additional terms that arise for input states that contain more than one photon per mode. The contributions of these terms are analysed for the device often referred to as both the Hong-Ou-

* E-mail: boyd@optics.rochester.edu

Journal of Modern Optics ISSN 0950–0340 print/ISSN 1362–3044 online
http://www.tandf.co.uk/journals
DOI: 10.1080/09500340110090819

Mandel interferometer [11, 12] and the quantum lithography [9, 10] configuration for input light derived from an optical parametric amplifier in both the low- and high-gain limits. For comparison, input beams in the form of coherent states of light are also considered. While a multiple-photon input can have significant effects on interferometer visibility, we find that desirable quantum statistical properties are preserved in the case of quantum lithography but are lost in the case of the Hong-Ou-Mandel interferometer (HOMI).

2. Low- and high-gain contributions to the joint detection rate

A four-port interferometer can generate coincidence counts at its exit via the four paths shown in figure 1. While explicitly depicting a Hong-Ou-Mandel interferometer, the diagrams and the following discussion are readily applied to any four-port interferometer. There are two types of paths shown in figure 1 for coincidence count detection: single-input paths, in which both detected photons arise from the same input arm, and dual-input paths, in which each input arm contributes one photon. Paths (a) and (b) are dual-input paths and differ only in the specific mapping of the input arms onto the output arms. These paths are the

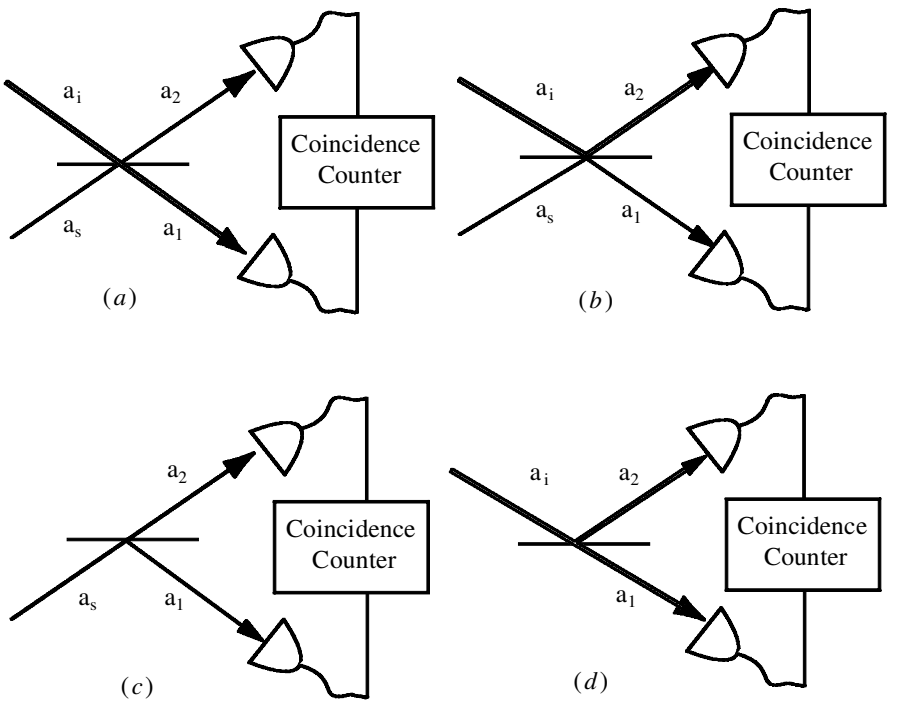

Figure 1. Processes contributing to the coincidence count rate. These diagrams represent symbolically the first four terms in equation (2). Processes (*a*) and (*b*) contribute in both the low-gain limit (that is, the spontaneous parametric downconverter) and high-gain limit of the output of an optical parametric amplifier. Processes (*c*) and (*d*) cannot contribute in the low gain limit in which there is only one photon in the input mode. The vacuum input from the open port in (*c*) and (*d*) does not contribute to the count rate as the detection system measures only normally ordered correlation functions.

only paths present when the input is a biphoton. The single-input paths (c) and (d) are present when multiple-photon inputs are used. These paths are not present with a biphoton input and, when introduced by increasing the gain of the OPA, contribute to a degradation of visibility in the Hong-Ou-Mandel and quantum lithography configurations.

For an interferometer governed by the relationships

$$\begin{pmatrix} \hat{a}_1 \\ \hat{a}_2 \end{pmatrix} = \begin{pmatrix} A & B \\ C & D \end{pmatrix} \begin{pmatrix} \hat{a}_s \\ \hat{a}_i \end{pmatrix}, \tag{1}$$

where $\hat{a}_s$ and $\hat{a}_i$ are the input signal and idler modes and $\hat{a}_1$ and $\hat{a}_2$ are output modes, the joint detection probability, assuming ideal, unit-quantum efficiency detectors, is given by

$$\begin{aligned} \langle \hat{a}_1^\dagger \hat{a}_2^\dagger \hat{a}_2 \hat{a}_1 \rangle = {} & |C|^2|A|^2\langle \hat{a}_s^\dagger \hat{a}_s^\dagger \hat{a}_s \hat{a}_s \rangle + |D|^2|A|^2\langle \hat{a}_s^\dagger \hat{a}_i^\dagger \hat{a}_i \hat{a}_s \rangle \\ & + |C|^2|B|^2\langle \hat{a}_i^\dagger \hat{a}_s^\dagger \hat{a}_s \hat{a}_i \rangle + |D|^2|B|^2\langle \hat{a}_i^\dagger \hat{a}_i^\dagger \hat{a}_i \hat{a}_i \rangle \\ & + 2\,\mathrm{Re}\; A^*C^*DA\langle \hat{a}_s^\dagger \hat{a}_s^\dagger \hat{a}_i \hat{a}_s \rangle + 2\,\mathrm{Re}\; A^*C^*CB\langle \hat{a}_s^\dagger \hat{a}_s^\dagger \hat{a}_s \hat{a}_i \rangle \\ & + 2\,\mathrm{Re}\; A^*C^*DB\langle \hat{a}_s^\dagger \hat{a}_s^\dagger \hat{a}_i \hat{a}_i \rangle + 2\,\mathrm{Re}\; A^*D^*CB\langle \hat{a}_s^\dagger \hat{a}_i^\dagger \hat{a}_s \hat{a}_i \rangle \\ & + 2\,\mathrm{Re}\; A^*D^*DB\langle \hat{a}_s^\dagger \hat{a}_i^\dagger \hat{a}_i \hat{a}_i \rangle + 2\,\mathrm{Re}\; B^*C^*DB\langle \hat{a}_i^\dagger \hat{a}_s^\dagger \hat{a}_i \hat{a}_i \rangle. \end{aligned} \tag{2}$$

The expectation values present in the first four terms correspond to the individual contributions of the four paths shown in figure 1. The remaining six terms arise from interference between two of these paths; for many input states most of these terms vanish.

This situation is summarized in table 1, which shows each of these quantum expectation values for various input states. For the biphoton input state $|11\rangle$ generated by spontaneous parametric downconversion, all of the interference terms are zero except for the term generated by the interference of the two paths in which one signal and one idler photon are detected. Furthermore, for a biphoton input, the first and fourth terms, corresponding to the single-input paths, are also zero as they require at least two photons in one of the input arms. We also note that all of the terms are present if coherent state inputs are used. In the quantum lithography configuration, we will see that the presence of these additional terms with coherent state input leads to components with undesired wider fringe spacing. The last column in table 1, labelled OPA, refers to the output of an unseeded optical parametric amplifier (OPA). The expectation values given in this table were calculated through use of the standard transfer relations of an OPA

$$\hat{a}_s = U\hat{a}_{s,0} + V\hat{a}_{i,0}^\dagger \tag{3}$$

$$\hat{a}_i = U\hat{a}_{i,0} + V\hat{a}_{s,0}^\dagger, \tag{4}$$

where U and V are parameters that describe the strength of the nonlinear interaction. It can be shown that the mean number of photons $\bar{m}$ in either of the arms has the value $|V|^2$; the quantum expectation values given in table 1 for the OPA are expressed in terms of this quantity.

Table 1. Quantum expectation values of the individual contributions (listed at the left along with their diagrammatic representations) to the joint detection probability $\langle \hat{a}_1^\dagger \hat{a}_2^\dagger \hat{a}_2 \hat{a}_1 \rangle$ of equation (2) for several different types of input states. Here $|mm\rangle$ designates the situation in which exactly m photons fall onto each input port, $|\alpha_0\alpha_0\rangle$ the situation in which the same coherent state falls onto each input port, and OPA the situation in which the signal and idler beams from an unseeded optical parametric amplifier are used as inputs.

		$\|11\rangle$	$\|m\ m\rangle$	$\|\alpha_0\alpha_0\rangle$	OPA
	$\langle a_s^\dagger a_s^\dagger a_s a_s \rangle$	0	$m(m-1)$	$\|\alpha_0\|^4$	$2(\bar{m})^2$
	$\langle a_s^\dagger a_i^\dagger a_i a_s \rangle$	1	m^2	$\|\alpha_0\|^4$	$2(\bar{m})^2 + \bar{m}$
	$\langle a_i^\dagger a_s^\dagger a_s a_i \rangle$	1	m^2	$\|\alpha_0\|^4$	$2(\bar{m})^2 + \bar{m}$
	$\langle a_i^\dagger a_i^\dagger a_i a_i \rangle$	0	$m(m-1)$	$\|\alpha_0\|^4$	$2(\bar{m})^2$
	$\langle a_s^\dagger a_s^\dagger a_i a_s \rangle$	0	0	$\|\alpha_0\|^4$	0
	$\langle a_s^\dagger a_s^\dagger a_s a_i \rangle$	0	0	$\|\alpha_0\|^4$	0
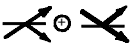	$\langle a_s^\dagger a_s^\dagger a_i a_i \rangle$	0	0	$\|\alpha_0\|^4$	0
	$\langle a_s^\dagger a_i^\dagger a_s a_i \rangle$	1	m^2	$\|\alpha_0\|^4$	$2(\bar{m})^2 + \bar{m}$
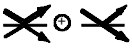	$\langle a_s^\dagger a_i^\dagger a_i a_i \rangle$	0	0	$\|\alpha_0\|^4$	0
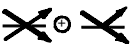	$\langle a_i^\dagger a_s^\dagger a_i a_i \rangle$	0	0	$\|\alpha_0\|^4$	0


single-input terms = both detached photons arise from a single input arm
dual-input terms = detected photons arise from both input arms

3. Effect of multiphoton input states on interferometer output

The value of the joint detection probability $\langle \hat{a}_1^\dagger \hat{a}_2^\dagger \hat{a}_2 \hat{a}_1 \rangle$ depends also on the interferometer-dependent coefficients that appear in equation (2) (e.g. $|C|^2|A|^2$ which multiplies $\langle \hat{a}_s^\dagger \hat{a}_s^\dagger \hat{a}_s \hat{a}_s \rangle$). The values of these coefficients for various interferometers are shown in table 2. In the case of an OPA, the 'interferometer' is simply the direct mapping of the signal to output 1 and the idler to output 2, that is, $A = D = 1$, $B = C = 0$. For the HOMI, the transfer matrix elements are given by

$$A = D = \frac{1}{\sqrt{2}} \tag{5}$$

$$B = C = \frac{-\mathrm{i}}{\sqrt{2}} \tag{6}$$

and for the quantum lithography configuration the matrix elements are given by

Table 2. For three different situations (listed at the top) the interferometer-dependent coefficient for each contribution (listed at the left along with its diagrammatic representation) to equation (2) is given. OPA refers to the joint detection probability measured at the output of an optical parametric amplifier, HOMI refers to the joint detection probability measured at the output of a 50/50 beamsplitter, and QL refers to the two-photon absorption rate at the recording plane in a quantum lithography configuration.

		OPA	HOMI	QL
	$\|C\|^2\|A\|^2$	0	1/4	$(1+\sin\chi)^2$
	$\|D\|^2\|A\|^2$	1	1/4	$1-\sin^2\chi$
	$\|C\|^2\|B\|^2$	0	1/4	$1-\sin^2\chi$
	$\|D\|^2\|B\|^2$	0	1/4	$1-\sin\chi)^2$
	2 Re A*C*DA	0	0	$2\cos\chi(1+\sin\chi)$
	2 Re A*C*CB	0	0	$2\cos\chi(1+\sin\chi)$
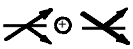	2 Re A*C*DB	0	1/2	$2\cos^2\chi$
	2 RE A*D*CB	0	$-1/2$	$2(1-\sin^2\chi)$
	2 RE A*D*DB	0	0	$2\cos\chi(1-\sin\chi)$
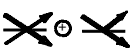	2 RE B*C*DB	0	0	$2\cos\chi(1-\sin\chi)$


single-input terms = both detached photons arise from a single input arm
dual-input terms = detected photons arise from both input arms

$$A = C = \frac{1}{\sqrt{2}} - \frac{\mathrm{i}}{\sqrt{2}}\mathrm{e}^{\mathrm{i}\chi} \tag{7}$$

$$B = D = -\frac{\mathrm{i}}{\sqrt{2}} + \frac{1}{\sqrt{2}}\mathrm{e}^{\mathrm{i}\chi}, \tag{8}$$

where χ is a phase angle proportional to the transverse coordinate across the substrate. It should be noted that in the quantum lithography configuration, the joint detection probability is related to the dose rate at a two-photon absorbing substrate rather than to a traditional coincidence count detection system. Note also that since the two outputs of the beamsplitter are combined on the lithographic plate, the relevant field modes $\hat{a}_1$ and $\hat{a}_2$ of the general theory are identical in this case, i.e. $\hat{a}_1 = \hat{a}_2$.

In the case of a measurement made directly at the outputs of an optical parametric amplifier, equation (2) reduces to $\langle \hat{a}_s^\dagger \hat{a}_i^\dagger \hat{a}_i \hat{a}_s \rangle$, which is simply the joint detection probability for the signal and idler modes. From table 1, we can see that, as expected, the joint detection rate from the parametric amplifier is increased over

the level produced by coherent state input. The second column in table 2 shows the Hong-Ou-Mandel interferometer coefficients. The negative sign on the dual-input interference term coefficients reflects the phase relationship that allows quantum interference to reduce the observed coincidence count rate. The single-input interference term coefficient is also nonzero; however, the expectation value $\langle \hat{a}_s^\dagger \hat{a}_s^\dagger \hat{a}_i \hat{a}_i \rangle$ that multiples this coefficient is zero for parametric amplifier outputs at both biphoton and high-gain levels. For coherent state input this term is present and leads to a net coincidence rate that shows no interference properties. The quantum lithography coefficients, shown in the last column of table 2, are all non-zero and phase dependent. Thus states with different dual- and single-input contributions can have net dose patterns that vary in spatial frequency as well as overall magnitude.

The joint detection probability for the Hong-Ou-Mandel interferometer is seen from table 2 to be given by

$$\langle \hat{a}_1^\dagger \hat{a}_2^\dagger \hat{a}_2 \hat{a}_1 \rangle = \tfrac{1}{4}[\langle \hat{a}_s^\dagger \hat{a}_s^\dagger \hat{a}_s \hat{a}_s \rangle + \langle \hat{a}_s^\dagger \hat{a}_i^\dagger \hat{a}_i \hat{a}_s \rangle + \langle \hat{a}_i^\dagger \hat{a}_s^\dagger \hat{a}_s \hat{a}_i \rangle + \langle \hat{a}_i^\dagger \hat{a}_i^\dagger \hat{a}_i \hat{a}_i \rangle] + \tfrac{1}{2}[\langle \hat{a}_s^\dagger \hat{a}_s^\dagger \hat{a}_i \hat{a}_i \rangle - \langle \hat{a}_s^\dagger \hat{a}_i^\dagger \hat{a}_s \hat{a}_i \rangle] \tag{9}$$

and gives the following results for each of the states considered. For a biphoton input, $\langle \hat{a}_1^\dagger \hat{a}_2^\dagger \hat{a}_2 \hat{a}_1 \rangle = 0$. For the same Fock state in each input arm, the joint detection probability is $\frac{1}{2}m(m-1)$, and for an optical parametric amplifier (OPA) input the joint detection probability is $\bar{m}^2$. Figure 2 shows this result for an OPA input with the contributions of the single- and dual-input terms displayed separately. The dual-input terms combine to give a net probability of zero; these are the only terms present for a biphoton input, leading to the coincidence count cancellation that is the hallmark of the Hong-Ou-Mandel interferometer. The single-input terms that become dominant as the photon number increases lead to a joint detection probability of $\bar{m}^2$ for the parametric amplifier. We note that this result has the same form as the probability for a coherent state input $\langle \hat{a}_1^\dagger \hat{a}_2^\dagger \hat{a}_2 \hat{a}_1 \rangle = |\alpha_0|^4 = \bar{m}^2$, with both being equal to the product of the single detector probabilities. Inspection of tables 1 and 2 shows that this apparent similarity arises through the contribution of different terms in each case.

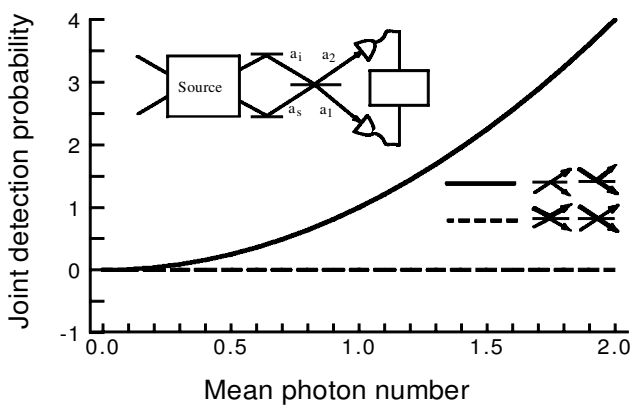

Figure 2. Single-input (———) and dual-input (- - - - -) contributions to the output of a Hong-Ou-Mandel interferometer. The dual-input contribution vanishes at all values of the mean photon number.

While the interplay of the interferometer coefficients and the states' expectation values lead to similar results with coherent and parametric amplifier inputs for the HOMI, the different weightings for each state present in the quantum lithography case lead to qualitatively different results for the parametric amplifier and coherent output states, even at high gain. The joint detection probability (that is, the two-photon absorption rate) for the quantum lithography configuration of figure 3 is given by

$$\begin{aligned}\langle \hat{a}_1^\dagger \hat{a}_2^\dagger \hat{a}_2 \hat{a}_1 \rangle = {} & (1+\sin^2\chi)[\langle \hat{a}_s^\dagger \hat{a}_s^\dagger \hat{a}_s \hat{a}_s \rangle + \langle \hat{a}_i^\dagger \hat{a}_i^\dagger \hat{a}_i \hat{a}_i \rangle] \\ & + (1-\sin^2\chi)[\langle \hat{a}_s^\dagger \hat{a}_i^\dagger \hat{a}_i \hat{a}_s \rangle + \langle \hat{a}_i^\dagger \hat{a}_s^\dagger \hat{a}_s \hat{a}_i \rangle + 2\langle \hat{a}_s^\dagger \hat{a}_s^\dagger \hat{a}_i \hat{a}_i \rangle + 2\langle \hat{a}_s^\dagger \hat{a}_i^\dagger \hat{a}_s \hat{a}_i \rangle] \\ & + 2\sin\chi[\langle \hat{a}_s^\dagger \hat{a}_s^\dagger \hat{a}_s \hat{a}_s \rangle - \langle \hat{a}_i^\dagger \hat{a}_i^\dagger \hat{a}_i \hat{a}_i \rangle] \\ & + 2\cos\chi[\langle \hat{a}_s^\dagger \hat{a}_s^\dagger \hat{a}_i \hat{a}_s \rangle + \langle \hat{a}_s^\dagger \hat{a}_s^\dagger \hat{a}_s \hat{a}_i \rangle + \langle \hat{a}_s^\dagger \hat{a}_i^\dagger \hat{a}_i \hat{a}_i \rangle + \langle \hat{a}_i^\dagger \hat{a}_s^\dagger \hat{a}_i \hat{a}_i \rangle] \\ & + 2\sin\chi\cos\chi[\langle \hat{a}_s^\dagger \hat{a}_s^\dagger \hat{a}_i \hat{a}_s \rangle + \langle \hat{a}_s^\dagger \hat{a}_s^\dagger \hat{a}_s \hat{a}_i \rangle - \langle \hat{a}_s^\dagger \hat{a}_i^\dagger \hat{a}_i \hat{a}_i \rangle - \langle \hat{a}_i^\dagger \hat{a}_s^\dagger \hat{a}_i \hat{a}_i \rangle] \qquad (10)\end{aligned}$$

and reduces to $\langle \hat{a}_1^\dagger \hat{a}_2^\dagger \hat{a}_2 \hat{a}_1 \rangle = 4(1-\sin^2\chi)$ for a biphoton input, $(1+\sin^2\chi)[2m(m-1)] + (1-\sin^2\chi)[4m^2]$ for a $|mm\rangle$ input, and $(1+\sin^2\chi)\ [4\bar{m}^2] + (1-\sin^2\chi)[8\bar{m}^2 + 4\bar{m}]$ for a parametric amplifier input, where the terms proportional to $1+\sin^2\chi$ arise from the single-input paths and the $1-\sin^2\chi$ terms arise from the dual-input paths. Figure 4 shows the parametric amplifier joint detection probability, with the relative size of the single-input versus the dual-input contribution plotted as a function of mean photon number. Recalling that the optimum visibility of unity is achieved with a biphoton input which has no single-input contribution, it is seen that, as the single-input contribution increases relative to the dual-input contribution, the visibility decreases to its limiting value of 1/5.

For each of the states generated by parametric downconversion, only terms that oscillate at twice the phase difference are present. The absence of terms oscillating as χ indicate that the patterns produced will have periods smaller than the Rayleigh limit without undesired slower terms. This is in contrast to the probability produced by coherent state inputs $\langle \hat{a}_1^\dagger \hat{a}_2^\dagger \hat{a}_2 \hat{a}_1 \rangle = \{2(1+\sin^2\chi) + 6(1-\sin^2\chi) + 8\cos\chi\}|\alpha_0|^4$. While the 'fast' $\sin^2\chi$ terms are present, the $\cos\chi$ term indicates the presence of undesired slower frequencies.

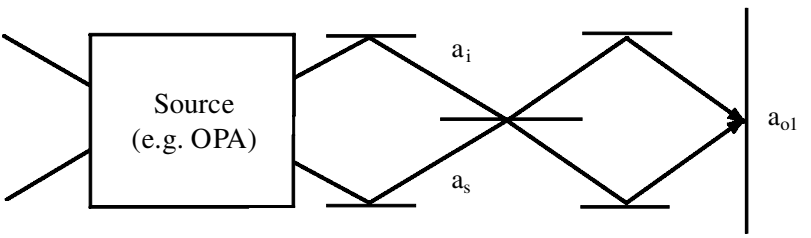

Figure 3. Quantum lithography configuration. The interference pattern is detected via two-photon absorption in the recording plane rather than by coincidence count detection. The resulting fringes have half the classical spacing

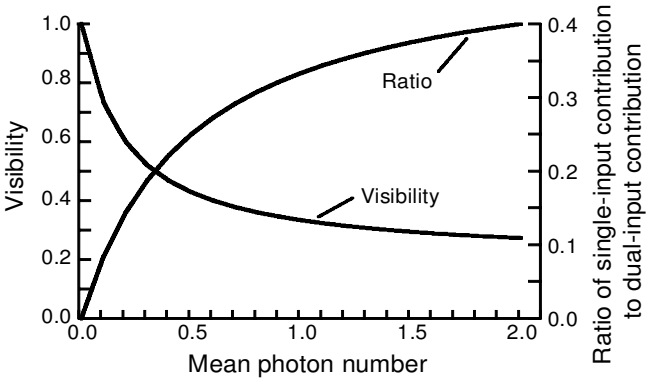

Figure 4. Visibility of the two-photon interference pattern of the quantum lithography configuration plotted as a function of the mean number of photons per mode at the output of the OPA. The visibility decreases as the relative contribution of the single-input terms increases.

4. Discussion and summary

In this paper, the single-input and dual-input contributions to the output of a four-port interferometer have been analysed in the context of the Hong-Ou-Mandel interferometer and quantum lithography. Single-input terms, which arise only with multiphoton states such as $|mm\rangle$, cause a degradation of desired interferometric properties such as high visibility, but properties such as sub-Rayleigh-limit resolution are preserved even when these terms contribute significantly to the overall output.

Acknowledgments

This work was supported by ARO grant DAAD19-01-1-0623, ONR grant N00014-99-1-0539, and NSF grant INT97-12760.

References

[1] Slusher, R. E. *et al.*, 1985, *Phys. Rev. Lett.*, **55,** 2409.
[2] Lugiato, L. A., 1996, *Phil. Trans. R. Soc. London A*, **354,** 767.
[3] Kolobov, M. I., 1999, *Rev. Mod. Phys.*, **71,** 1539.
[4] Vaupel, M., Maitre, A., and Fabre, C., 1999, *Phys. Rev. Lett.*, **83,** 5278.
[5] Souto Ribeiro, P. H., Schwob, C., Maitre, A., and Fabre, C., 1997, *Opt. Lett.*, **22,** 1893.
[6] Gatti, A., Brambilla, E., Lugiato, L. A., and Kobolov, M. I., 1999, *Phys. Rev. Lett.*, **83,** 1763.
[7] Fabre, C., Fouet, J. B., and Maitre, A., 2000, *Opt. Lett.*, **25,** 76.
[8] Gatti, A., Lugiato, L. A., Oppo, G.-L., Martin, R., Di Trapani, P., and Berzanskis, A., 1997, *Optics Express*, **1,** 21.
[9] Boto, A. N., Kok, P., Abrams, D. S., Braunstein, S. L., Williams, C. P., and Dowling, J. P., 2000, *Phys. Rev. Lett.*, **85,** 2773.
[10] Agarwal, G. S., Boyd, R. W., Nagasako, E. M., and Bentley, S. J., 2001, *Phys. Rev. Lett.*, **86,** 1389; Nagasako, E. M., Bentley, S. J., Boyd, R. W., and Agarwal, G. S., 2001, *Phys. Rev.* A., **64,** 043802.

[11] Alley, C. O., and Shih, Y. H., 1986, in *Proceedings of the Second Symposium on Foundations of Quantum Mechanics in Light of New Technology*, edited by M. Namiki *et al.* (Physical Society of Japan), p. 47; Shih, Y. H., and Alley, C. O., 1988, *Phys. Rev. Lett.*, **61,** 2921.
[12] Hong, C. K., Ou, Z. Y., and Mandel, L., 1987, *Phys. Rev. Lett.*, **59,** 2044.
[13] Saleh, B. E. A., Joobeur, A., and Teich, M. C. 1998, *Phys. Rev. A*, **57,** 3991.
[14] Shapiro, J. H., and Wong, N. C., 2000, *J. Opt. B: Quantum Semiclass. Opt.*, **2,** L1–L4.